Chaotic Modeling and Simulation (CMSIM) 3: 261-269, 2014

Spatial and temporal imaging of a plasma jet plume

V J Law[1*], L J Cox[2], W Adress[2], W G Graham[2] and D P Dowling[1]

[1]School of Mechanical and Materials Engineering, University College Dublin, Belfield, Dublin 4, Ireland.
[2]Centre for Plasma Physics, Queen's University of Belfast, Belfast, BT7 INN, UK
*(e-mail: viclaw66@gmail.com)

Abstract: Cold atmospheric pressure plasma jets have been shown to exhibit considerable potential for use in plasma medicine applications such as in wound treatment. New pulsed atmospheric pressure plasma jets are being developed that have inherent plasma stability and low gas temperatures. This study examines a new digital enhancement technique to characterise the far field plasma plume and effluent region of the plasma. The digital technique provides spatial information that identifies possible gas treatment zones for medical applications. Using images from a fast a capture (10 μm second) ICCD camera the study shows the luminous plume extends up to 7 mm from the reactor exit nozzle and has a kinked, or wrinkled, appearance but nonluminous perturbation of the gas is detected up to 3 cm away to the front and either side of the visible plasma plume.

Keywords: Imaging, Atmospheric plasma jet; Diagnostics.

1. Introduction

The development of the cold temperature atmospheric pressure plasma jets in recent years has led to the promising new science of plasma medicine. Treatments are generally applied using a hand-held atmospheric plasma sources that utilise a wide range of electric drive frequencies and reactor geometries. Examples of cell treatment leading to apoptosis using these plasma jets have been reported by a number of authors [1, 2]. One of the first clinically proven hand-held plasma jets is the kINPen med® developed by the Leibniz Institute for Plasma Science and Technology (INP), Greifswald, Germany in cooperation with neoplas GmbH, Greifswald, Germany is now undergoing in-vivo clinical investigation of plasma antiseptic properties on human skin [3], chronic venous leg ulcers [4] and cosmetic surgery [5]. These clinical trials require the relatively small 1.6 mm diameter plasma to treat large areas of thermally sensitive living tissue and microorganisms. Earlier studies using the kINPen 0.9 versions [6-8] of the plasma jet on microorganism have shown that cells are killed outside the visible plasma plume immediate treatment area, indicating

Received: 12 December 2013 / Accepted: 25 July 2014

ISSN 2241-0503

what has been termed a 'spillover' occurs [9]. Further to this, kINPen med® plasma induced activation studies on poly(ethylene-terephthalate) PET at a nozzle-to-surface distance of 5-15 mm have shown that a similar immediate activation (1 day) post treatment 'spillover' can be induced up to 20 mm in diameter on the polymer surface [10].

This work reports on the spatial and temporal visual imaging of the kINPen med® plasma plume fluid structure using a photodiode (PD) to trigger a gated ICCD camera, with the addition of a new digital image processing technique of the ICCD camera images. This post image processing technique is used to enhance the immediate area (up to a distance of approximately 3 cm) around the luminous plasma plume to reveal the fluid structure emanating from the gas flow. This digital image enhancement approach differs from the shadowgraph and Schlieren imaging technique previously for air/hydrogen jet [11], air discharge [12] and helium jets [13, 14] all of which probe the use of back lighting to probe the refractive index changes by density gradients in the fluid distortion Here no back lighting is required. This approach differs from the high temporal resolution flame-front visualization technique [15], and also differs from large time scale (10s) flow imaging of complex vortex mixing in DBDs [16]. In this work the widely available National Instrument LabVIEW software packages is used as an example.

2. Experiment apparatus and methods

Figure 1a shows a photograph of the plasma jet used in this study. The plasma reactor is a cylindrical dielectric barrier discharge made from a glass ceramic with an internal diameter of D = 1.6 mm. The inner metal electrode has a diameter of ~0.3 mm. The outer body is grounded to produce a cross-field jet configuration i.e. an electric field perpendicular to the gas flow. Here a gas flow rate of 5 SLM of 99.99% pure argon is used, equating to a gas velocity through the reactor tube of v = 36.7 $m.s^{-1}$. Since the plasma region is 20 mm long there is a gas residence time of about 0.5 ms.

Figure 1: Photograph of the kINPen Med® plasma interacting with a fingertip.

The inner electrode is powered by a 1 MHz electrical drive frequency that is

pulse modulated with 2.5 kHz square wave (50 % duty cycle) signal [10]. In this work the plasma plume, and effluent expands unobstructed into atmospheric pressure air, and is investigated with a PD, fast imaging camera and post image capture enhancement technique to reveal the fluid structure around the plasma plume (0-30 mm) in front and to the side of the plume.

The PD used was a Hamamatsu MPPC with a rise time of 10 ns and spectral range between 320 and 900 nm [17]. The light was collected at right angles to the plume, 1 mm downstream of the nozzle exit, via a fibre optic with a collimating lens, the combination producing a focal area of 1 mm in diameter at a length of 6 mm from the lens: Thus making the interrogation area smaller than to the diameter of the jet discharge (~1.6 mm). The rising edge of the 2.5 kHz modulated plasma light is used to trigger the ICCD Camera.

The Andor iStar 334T ICCD camera is used to capture the plasma images. A 14 cm focal length glass lens focused the region from between 2 mm upstream to 20 mm downstream of the exit nozzle. Using this combination the overall optical chain (between camera and plasma-plume) is of the order of 2 m and the camera spectral range is restricted to 300 to 850 nm by the glass lens. The camera was triggered, via a delay generator, from the rising edge of the PD signal. Within the camera the images are processed using a false-colour scale from blue (low intensity) to yellow (high intensity) for maximum visual differentiation the gain was set to 2817 out of a maximum of 4095, where the final digital images are formatted as a 24-bit red-green-blue (RGB) JPEG (Joint Photographic Experts Group) with a N x N pixel array, where N = 1024. Through an initial survey of the pulse-on and pulse-off periods of plasma the ICCD was synchronised to the respective time periods.

The gas behaviour beyond the luminous plasma region is explored by using LabVIEW based software [18]. This software essentially extracts the lowest intensity colour plane (blue plane) from the original RGB image and then uses pixel resolution enhancement through digital filtering and a thresholding algorithm. Care is taken at each step to ensure that the morphology in the recorded data is not distorted by reference at each step to experimentally available information, and the goals of the operation and limitations of the algorithms. The final images were achieved using four standard sequential steps.

1. The 8-bit “blue” plane is selected from the original 24-bit RGB image.
2. A fast Fourier Transform (FFT) is then applied to this plane to convert the spatial information into its frequency domain. A low-pass filter is used to smooth the noise with a truncation process to remove any remaining high frequency component above the user defined cut-off point.
3. An inverse FFT is then applied to bring the frequency domain data back into the spatial domain.
4. A local Nibalck thresholding segmentation algorithm is then used to produce a binary image. In this operation the background particles are set to I = 0 (black) while setting fluid structure to a pixel value of I = 1 (white). The result of this process produces a black-and-white binary image that represents the fluid structure within the original blue image.

3. Results.

3.1 Visible plasma imaging

Figures 2 provide examples of 15 individual ICCD images sampled from 31 images obtained for the argon plasma. The images span from the beginning of the pulse at t = 0 μs to the end stages of the pulse at, t = 185 μs. With the gain fixed at 2817 each image has the same intensity scale and therefore their intensities may be compared directly. To add comparison a scale bar is displayed at the top of the figure. The figure shows a linear increase in the length of the plume between 0 μs to 40 μs and rapid decrease in length beyond 185 μs when the plume is almost completely gone. Apart from the earliest and latest times the plumes vary in visible length and exhibit a kinked or wrinkled structure along the length of each plume.

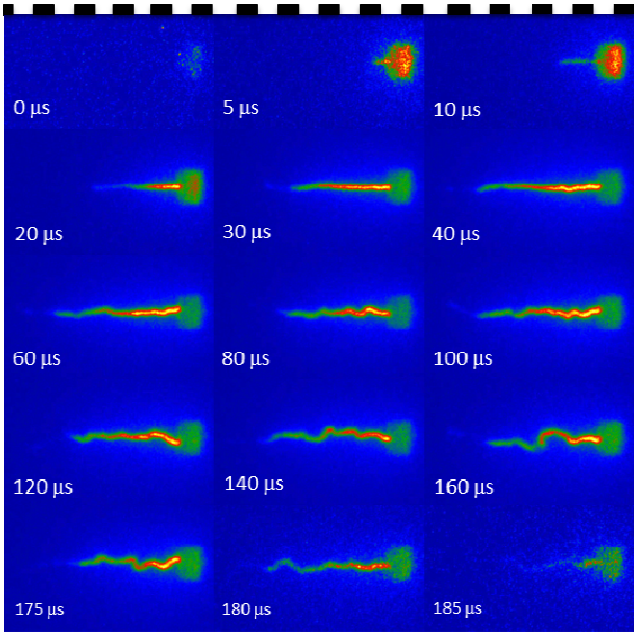

Figure 2: A selection (a total 15) of space and time resolved images of the nozzle and argon plasma.

Using all the 31 ICCD images, the distal length of each discharge plume have been calculated but are not shown here. The calculations reveal that the plasma expands from the nozzle and reaches, and maintains, a maximum length of about 4.5 or 6 mm until the voltage pulse is terminated. The initial velocity of the visible plume front is about 200 $m.s^{-1}$. However at about 4.25 mm the argon the front rapidly accelerates to about 300 $m.s^{-1}$ before reaching its maximum length with a periodic cycling ranging from 6.5 to 5 mm: with each cycle period taking 40 to 45 microseconds, which equates to a frequency of 20 to 22 kHz.

3.2 Spatial enhancement of non-visible plasma region

Figure 3 show a screen shot image of the LabVIEW colour plane extraction and line profile front panel for the pulse-on period. In this figure the left-hand images is the original 32-bit image with interactive line intensity profile (LIP) cursor; the second column of images are the three extracted blue, green and red planes (presented here in grayscale); the third column of graphs depict the selected LIP for each plane; and the final column is basic descriptive analysis of the LIP for each plane. The information presented on this front panel reveals that majority of the plasma information (white to grey colours) is aligned along the flow of the plume in the red and green planes. In contrast the far-field low intensity fluid structure information is captured within the blue plane as speckled noise surrounding the plume with an outer white ring at a typical distance of 2-4 plume diameters either side of the plume.

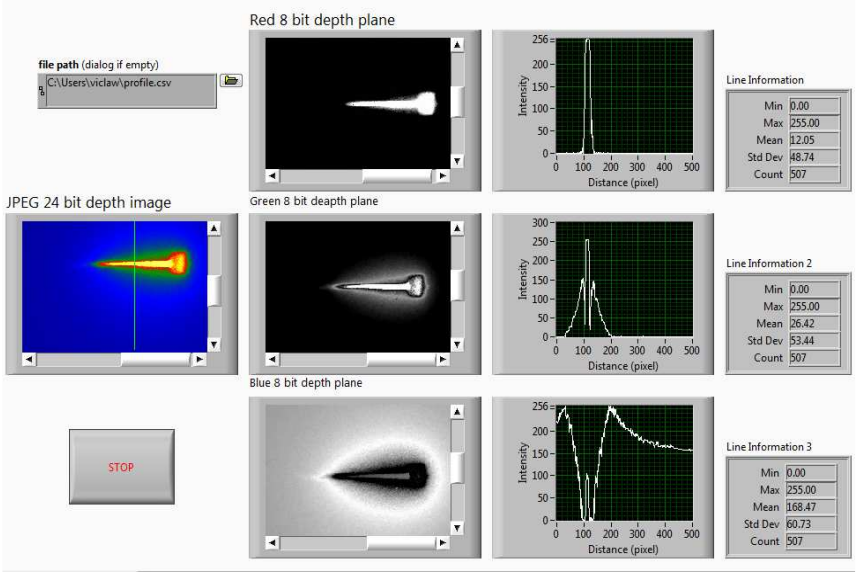

Figure 3: LabVIEW RGB colour plane and line profile.

We now turn to the digital filtering and threshold processing of the blue image. Figure 4 shows the processing of the duration of the pulse-on period and the duration of pulse-off period. It is interesting the structure observed on short time scale (figures 2) is absent in the long exposure image. It is also apparent from figure 4b that there is afterglow. In figure 4c we are imaging the structure of the background gas. This shows a distinct ripple-like feature centred in the proximity of the maximum light emission from the plume. Figure 4f show that this is absent when there is no discharge present.

To understand these fluid structure images we consider the dimensionless Reynolds number (R_e) as defined in equation 1 when interpreting figures 4c and 4f, as it provides a measure of the ratio of inertial forces to viscous forces and quantifies the relative importance of these two types of forces.

$$R_e = \frac{QD}{v_k A} \tag{1}$$

Where Q is the neutral argon flow rate (8.35 x 10-5 $m^3.s^{-1}$), D is the diameter of the nozzle (0.0016 m), v_k is the gas kinematic viscosity (0.000014 $m^2.s^{-1}$) and A is the cross sectional area of the nozzle (2 x 10^{-6} m^2). For argon gas flows of 5 SLM, R_e equates to 4465 which implies the inertial forces are expected to be more dominant than viscous forces and large-scale fluid motion would be un-damped in the pulse-off period. However when the plasma is turn-on, the neutral gas flow rate will increase due to the associated gas heating.

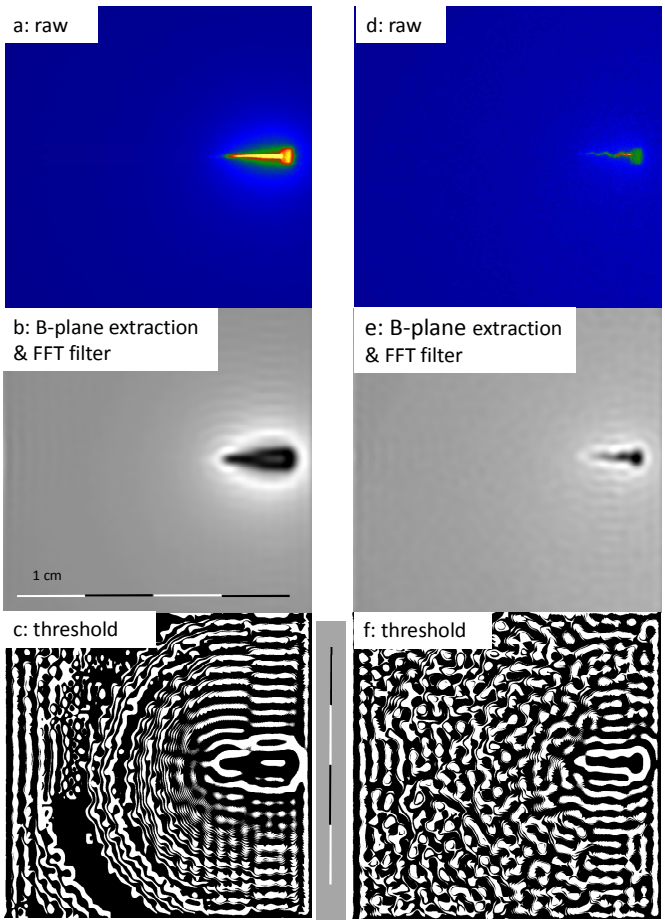

Figure 4: 0.2 μ second exposure ICCD images of plasma in pulse-on (a) and pulse-off period (d); images (b) and (c) depict the image enhancement of the pulse-on period; and images (e) and (f) depict the image enhancement for the pulse-off period.

Considering the processed image of the pulse-on period (figure 4c) a ripple structure is observed to radiate from a point along the axis of the plasma plume and extends with a complex structure in the direction of effluent flow up to 4 cm from the nozzle. This repeating far-field wave-like structure with a white peak distances separation of typically 1-2 mm is within an order of magnitude of the expected travel distance of the neutral gas within the capture time-frame of the camera image. In addition the ripple pattern is found to be asymmetric with respect to the effluent flow axis, producing a complex broken structures to the top beyond which the discontinuities the structures extend into the ambient air. The distance disturbance occurs at around 0.5 cm from the plume distal point.
In the case of the pulse-off period (figure 4f) the wave-like structures has collapsed to form irregular and small-scale chaotic structures with scale lengths of the order of the nozzle diameter. These observations are consistent with the Reynolds number dimensionless analysis and the loss of driving force to heat the plasma gas when the electrical drive power is switched-off. Under these conditions the heated gas is expected to begin to equilibrate with the surrounding ambient air. This imaging technique is also supported by the work of Roberts et al who have used the Schlieren technique to look at a pulsed helium jet. In their work they found. They found rapid changes in the stability at the start and end of the pulse period.

Using the work of Ghasemi *et al* [14], we can obtain, to a first approximation, the increase in gas velocity when the plasma is turn-on by using the continuing mass flow equation (2). In this equation: $\rho_{1,2}$ are the densities of the argon gas at room temperature (1.62 kg.m^3) and plasma temperature 1.47kg.m^3 (3*30 K* [1, 2]). A is the cross-sectional area of the jet nozzle and $V_{1,2}$ are the argon gas velocities at room temperature and plasma temperature, respectively.

$$\rho_1 A V_1 = \rho_2 A V_2 \tag{2}$$

Assuming the argon gas mass flow rate is the same in both case (5 SLM), the argon gas velocity increase from 41 m.s^{-1} at room temperature (~300 *K*) to 45 m.s^{-1} at the expected plasma temperature of ~33.0 *K*.

4. Conclusion

The spatial and temporal visual imaging of an argon-based pulsed plasma jet designed for medical use has been studied using photodiode and ICCD camera imaging, plus post exposure enhancement of the camera images. This combined measurement and diagnostic approach provides a spatial and temporal picture of the plasma plume and its effluent. The PD measurements show that the plasma is modulated by a fast rising and falling 2.5 kHz square wave time-base profile. Microsecond time scale imaging of the discharge using the ICCD camera reveals that the argon plasma plume is continuous through the 0.2 ms pulse-on period of the discharge. However the plume morphology takes on a kinked or wrinkled appearance. In addition the plume rapidly decays at the end of the

voltage pulse suggesting micro-turbulence is the driving force in the production of the kinks within the plasma jet.

To gain access to the effluent gas being expelled from the plasma plume the technique of image plane extraction has been developed and demonstrated. Here the blue plane of the ICCD digital images has revealed pulsed plasma induced fluid structures extending up to 2-3 cm form the visible plume. This far-field fluid structure information may be used in the understanding 'spillover' effect when plasma treating thermally sensitive polymers and their biomaterial counter parts.

Acknowledgement

L. J. Cox is supported by a grant from the Department of Education and Learning Northern Ireland, and W. Adress is supported by the Iraqi Ministry of Higher Education and Scientific Research. This work is part supported by Science Foundation Ireland Grant 08/SRC114; COST ACTION programme and; the 7th CHAOS2014 International Conference, Lisbon, Portugal organizing committee.

References

1. Georgescu. N, and Lupu. A R. Tumoral and normal cells treatment with high-voltage pulsed cold atmospheric plasma jets. IEEE. Trans. Plasma Sci. 38(8), 1945-1955, 2010.
2. Ahn. H. J, Kim. K Il, Moon. Kim. G, Yang. S. S, Lee. J-S. Atmospheric-pressure plasma jet induces apoptosis involving mitochondria via generation of free radicals. PluS One. Plasma Sci. 6(11), e28154 (7pp), 2011.
3. Lademann. J, *et al*. B. Risk assessment of the application of tissue-tolerable plasma on human skin. Clinical Plasma Medicine 1, 5-10, 2013.
4. Isbary. G, *et al*. Non-thermal plasma-More than five years of clinical experience. Clinical Plasma Medicine 1, 19-23, 2013.
5. Metelmann. H-R, *et al*. Experimental recovery of CO_2-laser skin lesions by plasma stimulation. American Journal of Cosmetic Surgery 29(1), 52-56, 2012.
6. Weltmann. K-D, *et al*. Atmospheric pressure plasma jet for medical therapy: plasma parameters and risk estimation, Contrib. Plasma Phys. 49(9) 631-64, 2009.
7. Daeschlein. G, *et al*. In vitro killing of clinical fungal strains by low temperature atmospheric pressure plasma jet, IEEE Trans. Plasma Sci. 39(2), 815-821, 2011.
8. Daeschlein. G, *et al*. Skin decontamination by low temperature atmospheric pressure plasma jet and dielectric barrier discharge plasma, J. Hosp. Infect. 81 177-183, 2012
9. Kolb. J. F, *et al*. Cold dc-operated air plasma jet for the inactivation of infectious microorganisms. IEEE Trans, Plasma Sci. 40(11), 3007-3026, 2012.
10. Law. V. J, *et al*. Resonances and patterns within the kINPen-MED

atmospheric pressure plasma jet. CMSIM Journal. 1, 3-10, 2014.
11. Carlsson. T. E, *et al*. Combination of schlieren and pulsed TV holography in the study of a high-speed flame jet. Optic and Lasers in Engineering. 44(6), 535–554, 2006.
12. Sutton. Y, Moore. J, Sharp. D, and Braithwaite. N. St. Looking into a plasma loudspeaker. IEEE Trans, Plasma Sci. 39(11), 2146-21487, 2011.
13. Ghasemi. M, Olszewski. P, Bradley. J. W, and Walsh. J. L. Interaction of multiple plasma plumes in an atmospheric pressure plasma jet array. J. Phys. D: Appl. Phys, 46, 052001 (6pp), 2013.
14. Roberts. E, Sarron. V, Darny. T, Ries. D, Dozias. S, Fontane J, Joly. L, and Pousvesle J-M. Rare gas flow structuration in plasma jet experiments. PSST. 22 012003 (5pp), 2014.
15. Wisman. D, and Ganguly. B. Flame-front visualization using argon–oxygen plasma discharge. IEEE Trans, Plasma Sci. 39(11), 2066-2067, 2011.
16. Dahai Yu, *et al*. Influence of a rotating electrode on the uniformity of an atmospheric pressure air filamentary barrier discharge. Plasma Process. Polym. 2013.
17. O'Neill. F. T, Twomey. B, Law. V. J, Milosavljević. V, Kong. M. G, Anghel. S. D, and Dowling. D. P. Generation of active species in a large atmospheric pressure plasma jet. IEEE Trans. Plasma Sci. 40(11) 2994-3004, 2012.
18. Law. V. J, O'Neill. F. T, and Dowling. D. P. Automatic computation of crossing points within orthogonal interpolation line graphs. *How nature works: Emergence, Complexity and Computation*. 195-216, Eds. I Zelinka, A. Sanayei, H. Zenil, and O. E. Rössler. (Springer International Publishing Switzerland 2013).